

I. Abstract

We have invented a method that results in the realization of a charge-coupled device (CCD) on a fully-depleted, 300 μm thick high resistivity n-type silicon substrate. The substrate is fully depleted by the application of an independent voltage through an optically transparent backside contact. As a consequence of these innovations the CCD has superior near infrared and blue response ($\lambda = 300$ to 1050 nm) over existing CCDs. The next generation of major science projects planned for all of the largest telescopes require large-format image sensors with high quantum efficiency continuously from 300nm to 1050nm. This CCD uniquely satisfies this requirement.

The optical absorption length in silicon increases dramatically with wavelength, changing by more than three orders of magnitude over the optical region. The typical CCDs in current use on a low-resistivity silicon substrate have a thin 20 μm active region, limiting optical sensitivity for $\lambda \gtrsim 850$ nm. For imaging applications, blue losses in the front circuitry are avoided by rear-illumination of “thinned” CCDs, in which the substrate under the active region has been removed. The process is time-consuming, has low-yield, and is costly. It also introduces a second reflecting surface, so that multiple reflections produce interference fringes at long wavelengths.

Previous CCDs on high-resistivity silicon, called “deep-depletion” devices, cannot achieve full depletion of a thick substrate, require thinning to 40-50 μm , and still suffer from fringing in the near IR. The alternative “full-depletion” technology radically departs from these previous CCDs and by virtue of the thick substrate yields high quantum efficiency while avoiding the costly “thinning” processes. The expected quantum efficiency of our “full-depletion” technology with a two layer anti-reflective coating is 85% at 1000nm (T=270K) while “deep-depletion” CCDs have achieved at best 16%. The use of an optical window with an applied depletion bias voltage also yields excellent blue response in the “full-depletion” technology. Consequently, these devices can provide wider wavelength sensitivity with higher quantum efficiency at lower cost than devices currently in use in astronomy.

The group has already fabricated and tested small (200×200 ($15 \mu\text{m}$)² pixels) back-illuminated CCDs on high-resistivity ($\sim 12 \text{ k}\Omega\text{-cm}$) n-type silicon, making use of a high-purity process to maintain very low leakage currents. Larger devices, up to $2K \times 2K$ are currently under test. These 300- μm thick devices operate totally depleted, with back illumination. They have outstanding near-infrared response to just beyond 1000 nm with no fringing, and excellent blue response without UV flooding or special processing. Experimental and theoretical studies verify that lateral diffusion is less than or comparable to that in existing devices. The conventional MOS processing implies an order of magnitude lower cost versus “thinned” CCDs.

II. Description

i. Introduction

Innovative imaging charge-coupled devices (CCDs) with superior red response (flat response to 1 μm with no fringing) are under development. The CCDs are made using standard MOS processing on high-resistivity n-type substrates and are operated fully depleted. Tests of small prototypes have verified the potential of the technology [1,2,3,4].

The new CCDs can be produced at low cost yet will have superior quantum efficiency over existing high cost CCDs including other MOS CCDs fabricated on high-resistivity silicon. This new technology will permit wideband imaging and spectroscopy from 300nm to 1050nm in low cost large area mosaic arrays ideally suited for planned science projects at all of the largest telescopes. Already superior quantum efficiencies have been achieved throughout the wavelength range of 300 nm to 1000 nm. Further significant improvements will be made as optical coatings are optimized and improved.

To overcome a variety of technical problems discussed below, high-performance CCDs for astronomy are obtained by “thinning” conventional CCDs (where the active region is a thin 30–50 Ωcm epitaxial layer grown on a lower-resistivity p-type substrate), leaving only the epitaxial layer and gate circuitry. After back-surface preparation they are used with back illumination. There are severe cost, quality, and availability problems associated with the process. For example, each of the four or more 2048×2048 pixel CCDs in a modern mosaic camera costs from \$50,000 to \$100,000, about an order of magnitude higher than the cost of the CCD as it leaves the foundry due to the cost and yield of the subsequent “thinning” process [5].

All of these problems are avoided by the UCB/LBNL technology, in which the final CCD emerges directly from the MOS foundry. There are additional gains: Since holes rather than electrons are collected, no special back-window treatment is necessary to achieve high blue sensitivity. These CCDs are likely to be more radiation resistant than standard CCDs, because boron, rather than phosphorus, is used for doping, and because the high-resistivity substrate contains comparatively little oxygen. Because they are thick, red sensitivity is extended to near the bandgap cutoff at 1100 nm ($T=150\text{K}$) [6]. No other MOS CCD process offers these improvements.

These “fully-depleted” 300 μm thick high-resistivity MOS CCDs are unique and exhibit significantly improved performance over existing “deep-depletion” CCDs which still require thinning to 40-50 μm for good performance and are technically quite different.

This new CCD evolved from technologies developed for high energy physics silicon vertex detectors which required radiation hardened pixelated detectors; however, the UCB/LBNL effort in this development was motivated by the needs of the UCB/LBNL-based Supernova Cosmology Project. The instrumental improvements essential to the group’s future work serve to illustrate the importance of the effort for optical astronomy in general.

The CCDs are developed, tested, and characterized at UCB and LBNL, and the CCD laboratory at UCO/Lick.

ii. Uniqueness of UCB/LBNL Technology

The technology under development at UCB/LBNL is innovative and unique. Key to the technology are: 1) use of lightly doped n-type high-resistivity substrates, 2) transistor devices for these substrates, 3) optically transparent ohmic contacts for the backside, 4) device structures enabling the application of the bias voltage and minimizing noise, leakage currents, and diffusion, and 5) development of CCD structures for operation on the n-type high-resistivity substrates.

A backside voltage is applied through an optically transparent contact while minimizing leakage currents such that the unthinned 300 μm thick substrate can be fully depleted. The application of an independent backside voltage required to deplete a thick substrate with a conventional MOS CCD is unique among CCD developers. The additionally required optically transparent ohmic contact is also unique. Consequently, the UCB/LBNL CCD is the only “fully-depleted” thick MOS CCD.

Full depletion of a standard low-resistivity silicon substrate is not technically feasible. So the technical developments for expanding the wavelength sensitivity of scientific CCDs have focussed on high-resistivity substrates. Unique among MOS CCD developers is the use at UCB/LBNL of a lightly doped high-resistivity n-type silicon substrate. The community of developers of MOS CCDs on high-resistivity silicon is small, limited to UCB/LBNL, MIT/Lincoln Laboratory [7,8,9], and EEV Ltd [10,11,12,13,14].

The MOS CCDs developed at MIT/Lincoln Labs and EEV Ltd. are of the “deep-depletion” type. In these devices partial depletion of the substrate is achieved to depths of typically 40-80 μm through the potential applied at the charge transfer gates. The devices must still be thinned to 40-50 μm in order to eliminate the field-free region between the depletion layer and the backside [7,10]. Thinning unfortunately undermines the long wavelength sensitivity and introduces large amplitude

interference fringes at long wavelengths. The need to apply the depletion potential at the charge transfer gate makes these devices harder to optimize.

The n-type substrate also avoids the backside electron-trapping which is a problem for all p-type material CCDs. The use of n-type material is also expected to result in improved resistance to bulk radiation damage due to the extremely low density of phosphorus in the CCD channel region [15]. Improved radiation resistance has already been observed in a proton test beam with fluences up to $1 \times 10^9 p/cm^2$.

The application of a substrate bias voltage to the backside window has several advantages for the “fully-depleted” CCDs. First, the potential developed by the CCD gate voltages is largely independent of the substrate bias, hence the CCD gate voltages can be set to optimize CCD parameters (well depth, CTE, etc...), while the substrate bias is used to set the depletion depth [3]. In a “deep-depletion” CCD the gate bias voltage determines the depletion depth for a given resistivity. Maximizing depletion depth via gate voltage can result in the degradation of other CCD parameters. Second, it allows for overdepletion with no significant increase in dark current. High resistivity wafers vary significantly in doping uniformity so there can be significant variation in depletion thickness across the device if not fully or overdepleted. The normal clock biasing will result in a depletion thickness variation in each pixel for the case of partial depletion [8]. Third, by overdepleting the CCD the absence of a field-free region can be guaranteed and the rate of charge spreading can be controlled.

Therefore, when compared to existing CCDs, the uniqueness of the LBNL CCD is summarized as follows:

1. The significantly lower dopant density used in the UCB/LBNL n-type substrates results in full depletion of 300 μm thick substrates at reasonable operating voltages.
2. The complicated and expensive thinning to 40-50 μm as required in existing “deep depletion” CCDs is eliminated.
3. The significantly thicker UCB/LBNL CCD has higher quantum efficiency in the near IR wavelength region when compared to “deep depletion” CCDs.
4. Related to 3), fringing in the red end of the spectrum is still a problem with existing “deep depletion” CCDs, and is for all practical purposes eliminated in the UCB/LBNL device.
5. The use of a unique substrate bias voltage results in independent control of depletion thickness, without compromising CCD operating parameters (versus when gate electrode bias is used to set the depletion depth as in existing “deep depletion” CCDs).
6. The use of n-type substrates eliminates the backside electron trapping problem and is expected to result in significantly improved radiation resistance.

The UCB/LBNL “fully-depleted” CCD utilizes conventional MOS technology. This implies that technology transfer to any of a number of CCD manufacturers is possible without the need for customized fabrication equipment to handle the double-sided lithography. The major difference for wafers used by UCB/LBNL compared to industry standard wafers is the thickness (300 μm versus industry standard 550 μm for 4 inch diameter). However, we have shown that conventional lithography tools used in CCD manufacturing can operate with both wafer thicknesses (demonstrated on both 1:1 scanners and 5:1 steppers). We have further identified a major CCD manufacturer able to process wafers of this thickness to our specifications. Consequently, the “fully-depleted” thick MOS CCDs will be inexpensive to manufacture due to the lack of thinning and backside lithography.

iii. Comparison of CCDs

The CCD design dilemma is summarized in Fig. 1. At the atmospheric cutoff at the blue end ($\lambda \approx 320$ nm), the absorption length of light in silicon is about 10 nm. It is four orders of magnitude larger, or 100 μm , at $\lambda = 1000$ nm. The problem at the blue end is to collect electrons

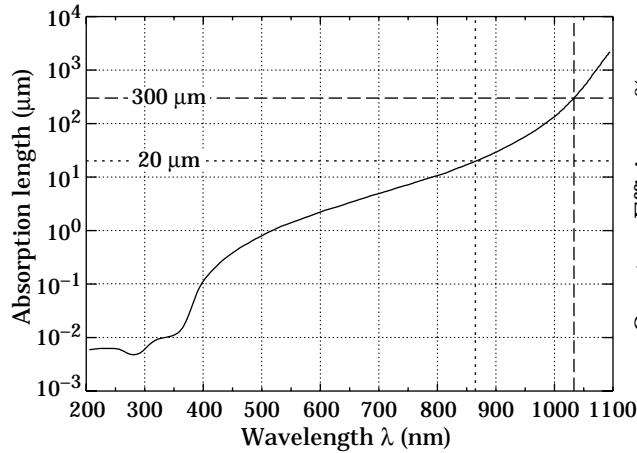


Figure 1: Absorption length of light in silicon (solid curve). Except at wavelengths approaching the bandgap cutoff at $\lambda_b \approx 1100$ nm, essentially all absorbed photons produce e-h pairs. The sensitive region of a conventional CCD is the ≈ 20 μm -thick epitaxial layer, indicated by the dotted line, while in the high-resistivity CCDs the fully-depleted 300 μm substrate is active (dashed line).

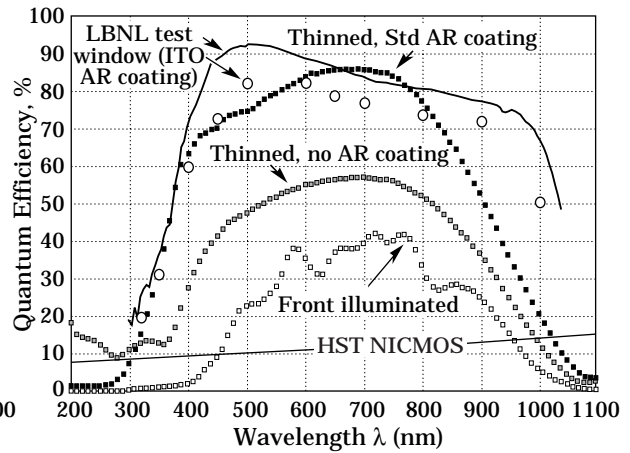


Figure 2: Quantum efficiencies (QEs) of conventional CCDs with front illumination, thinned with back illumination, and thinned, back-illuminated with an antireflective coating [26]. The solid curve is for a photodiode with a back window consisting of 10 nm polysilicon plus an indium-tin oxide (ITO) AR coating optimized for 400 nm [27]. The open circles are Lick measurements of a UCB/LBNL CCD with a 20 nm polysilicon + ITO window.

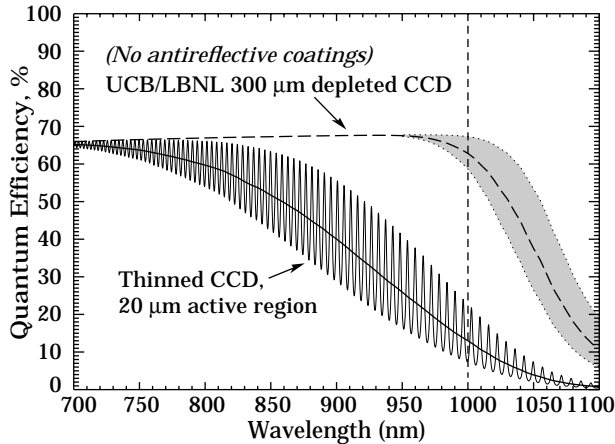


Figure 3: Calculated quantum efficiencies for thinned CCDs (20 μm thick) and UCB/LBNL CCDs (300 μm thick, totally depleted) for the case with no antireflective coating.

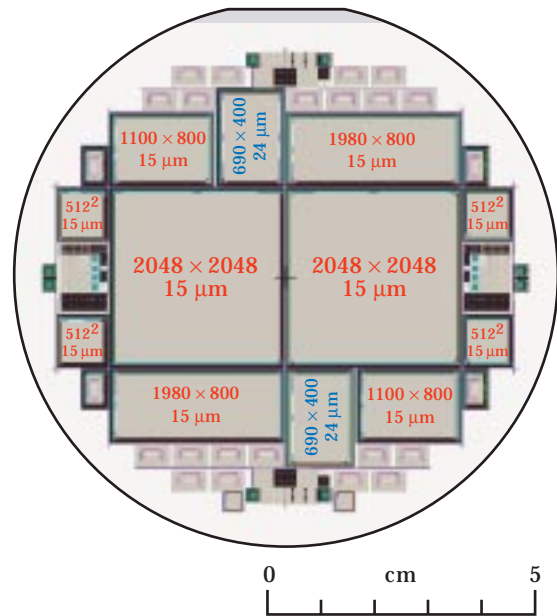


Figure 4: Mask design used for the next fabrication runs. Included in this design are CCDs varying in size from 200×200 to 2048×2048 , transistor test structures of varying geometry, p-i-n diode test structures, and a variety of process monitors.

(or holes, in the case of this work) produced very near the entrance window. At the red end, quantum efficiency (QE) decreases as the device becomes transparent. In the case of a thinned device, the loss of QE is accompanied by the production of interference fringes due to multiple reflections. Typical QEs for astronomical CCDs are shown in Fig. 2, along with measured QE for the UCB/LBNL prototype CCD. The solid curve is in good agreement with calculations under the assumption that all photons not reflected or transmitted are absorbed and produce detected holes.

The “fully-depleted” thick CCDs have a wider range of wavelength sensitivity than backside illuminated conventional CCDs or “deep-depletion” CCDs, including improved blue response due to the optical contact, and significantly better IR response. The best MIT/Lincoln Laboratory “deep-depletion” CCD is measured to have 16% quantum efficiency at 1000 nm [25] whereas our prototype device, with its single AR coating optimized for 400 nm, has a 50-67% quantum efficiency at 1000 nm (see Fig. 2). Future devices are expected to achieve 70%.

The absorption depth of near IR light is greater than $10\ \mu\text{m}$ for wavelengths greater than approximately 800 nm. Once the absorption depth reaches approximately half the thickness of the device interference fringing is expected (see Fig. 3). Since our device is so thick the problem of fringing (interference) which occurs in thinned devices is much ameliorated. The MIT/Lincoln Laboratory CCD has a fringing amplitude of 30% at 1000 nm [25] which reduces the utility of the devices for accurate spectroscopic measurements.

Calculated red response is shown in Fig. 3, where for simplicity no antireflective (AR) coating was assumed. The QE and interference patterns expected for thinned CCDs agree well with experiment. In the UCB/LBNL case fringing does not occur below 975 nm, and the fringes are about 15 times closer, so that they are washed out by the angular spread of the light in even moderately fast optical systems.

In Table 1 the characteristics of UCB/LBNL CCDs are given along with the performance characteristics of other competitive devices. One favored substitute for CCDs in the near-IR region are HgCdTe active pixel devices. A HgCdTe array is grown on a sapphire substrate, illuminated through the sapphire, and indium bump-bonded to silicon readout chips. This novel device has not yet been produced in quantities for large format mosaic instruments and remains very expensive.

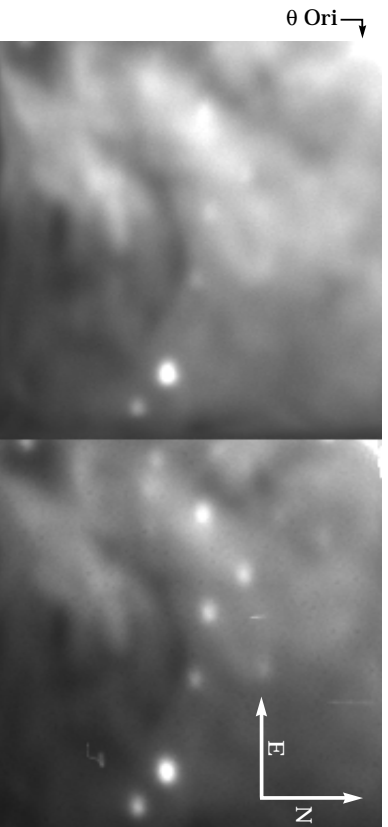


Figure 5: UCB/LBNL test CCD images of a heavily obscured region in the Orion Nebula, observed under poor conditions on 1996 Dec 4 with the Lick Observatory 1-m telescope on Mt. Hamilton. The left image was a 50 s exposure with a Harris R filter, with a peak transmission at 600 nm and a FWHM of 120 nm. The right image was a 100 s exposure through a special filter with maximum transmission at 1000 nm and FWHM 88 nm. Each field is about 57 arc-sec squared.

iv. Preliminary results from UCB/LBNL high-resistivity CCDs

Astronomical images using a 200×200 pixel back-illuminated high-resistivity CCD fabricated at UCB/LBNL were first obtained on 1996 Dec 4. In a test at the Lick Observatory 1 m telescope,

Table 1: Characteristics of UCB/LBNL 200×200 ($15 \mu\text{m}$)² test CCDs as compared with other red-sensitive detectors.

Characteristic	LBNL test	LBNL expected	Typical CCD [‡]	MIT/Lincoln*	HgCdTe [†]
Typical format	200×200	$2K \times 2K$	$2K \times 2K$	$2K \times 4K$	$2K \times 2K$
Operating Temp.	150 K	150 K	150 K	150 K	78 K
CTE	> 0.999999	> 0.999995	> 0.999995	> 0.999995	—
Read noise	4–6 e	4 e	3–6 e (best $\approx 1 e$)	2–4 e	4 e
Dark current	0.3 e /m/pix	0.3 e /m/pix	0.03 e /m/pix	0.03 e /m/pix	1 e /m/pix
Full-well (e 's)	240k–300k	240k–300k	150k (non-MPP)	120k	90k
Fringing @ 1000 nm	< 5%	< 5%	30%	30%	—
QE @ 1000 nm [◊]	50–67%**	70%	5–10%	10–16%	56%
Cost	—	8K	50–100K	—	300K

[‡] <http://sauron.as.arizona.edu/ccdlab/>

* <http://gardiner.ucolick.org:80/~ccdev/lincoln>

[†] Hawaii-2 array prospects/cost as reported by K. Hodapp [28], Q.E. is from Hawaii-1 array

[◊] At cold temperatures (T=150K) where QE drops due to bandgap widening [29].

** Single AR coating with best transmission at 400 nm. Range is difference between LBNL and Lick measurements

a heavily obscured region of the Orion Nebula was imaged using an R filter, which has maximum transmission near 600 nm, and a narrow bandpass 1000 nm filter obtained especially for these tests. The examples shown in Fig. 5 show stars obscured at 600 nm but which are visible at 1000 nm. Exposure times and image densities indicate comparable QE at each wavelength. To the best of our knowledge, this is the first demonstration of high-QE imaging at 1000 nm with a CCD.

In Table 1 the UCB/LBNL test CCDs are compared with other available detectors for the 700 nm–1000 nm wavelength region. Charge transfer efficiency (CTE), quantum efficiency (QE) as a function of wavelength, noise, and full well capacity, have been characterized on the 200×200 prototypes. As expected when compared to thinned CCDs the dark current is larger in the UCB/LBNL CCD by a factor of approximately the thickness ratio (larger volume for dark current generation in the substrate). The CCDs were characterized in detail at the Lick Observatory CCD Laboratory.

Charge transfer efficiency was measured on the 200×200 prototype, but the measurements were limited by the short baseline. Absolute CTE is measured using the line stacking technique with an ^{55}Fe source [30]. Recently a new CTE measurement technique was applied to the 200×200 , and values of greater than 0.999999 were measured [31].

Based on the success of the 200×200 ($15 \mu\text{m}$)²-pixel prototype [1,2,3,31], the case for developing large area CCDs suitable for scientific imaging applications is very compelling. It is clear that the device is already superior for optical astronomy except for its small size.

v. Technical features of high-resistivity CCDs

Figure 6 shows the basic concept for the back-illuminated, fully-depleted CCD. A conventional three-phase, buried-channel CCD is fabricated on a high-resistivity silicon substrate of nominal thickness 300 μm . A bias voltage is applied to the backside contact in order to fully deplete the

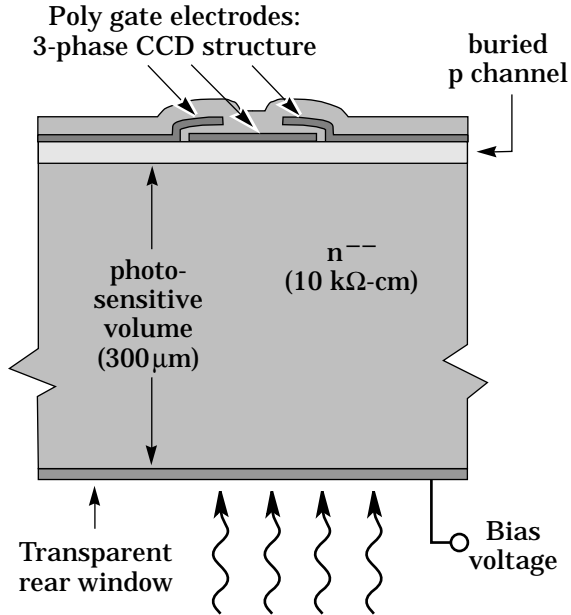


Figure 6: Cross-sectional drawing of the back-illuminated, fully-depleted CCD. A conventional buried channel CCD is fabricated on a high-resistivity silicon substrate. A bias voltage applied to the backside contact results in full depletion of the substrate.

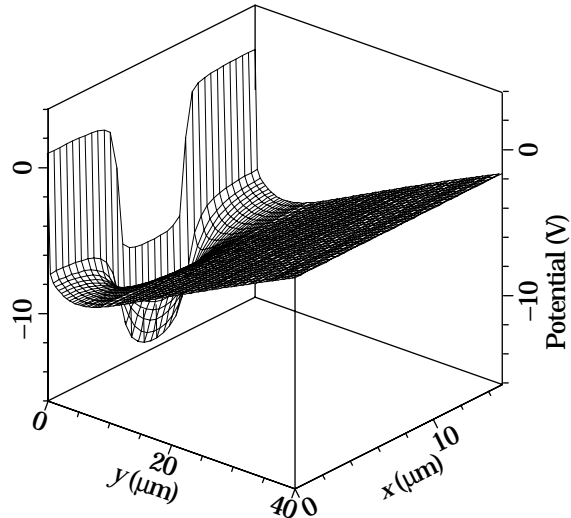


Figure 7: Simulated potential distribution for the cross-section shown in Figure 6. The substrate doping was $6 \times 10^{11} \text{ cm}^{-3}$ and the buried channel implant dose was $1.5 \times 10^{12} \text{ cm}^{-2}$. The origin in Y corresponds to the top of the buried channel region in Figure 6.

300 μm thick substrate. This contact is also the illumination entrance window. An antireflective coating is added to maximize transmission over the extended optical region, 300 nm–1000 nm.

The use of a high-resistivity substrate permits fully depleted operation at reasonable bias voltages. The effect of the bias voltage is to remove the mobile electrons resulting from the extremely small number of dopants atoms (phosphorus) in the high-resistivity silicon. The resistivity of $\approx 10,000 \text{ } \Omega\text{-cm}$ corresponds to a doping density in the mid- 10^{11} cm^{-3} range, about four orders of magnitude smaller than in conventional CCDs. The substrate thickness used here, 300 μm , is significantly thicker than previous conventional, deep-depletion CCDs with typically 40-80 μm thick depletion regions [7,8,9,10,11,12,13,14,32,33].

The removal of the mobile electrons from the substrate results in an electric field due to the dopant atoms that are now ionized and positively charged. This electric field extends essentially all the way to the backside contact, hence the term full depletion. This element is key to the proper operation of the back illuminated CCD. Short wavelength light is absorbed very near the backside contact. In order to minimize the loss of spatial resolution due to thermal diffusion, it is important the the photo-generated charge be directed towards the CCD buried channels by an electric field. If any significant field-free region is present, the spatial resolution will be significantly degraded by charge diffusion. This is discussed in more detail below.

Figure 7 shows the results of a two-dimensional simulation [34] of the CCD structure shown in Figure 6. Bias voltages on the polycrystalline silicon gates result in a potential well where the photo-generated charge carriers are collected. A drift electric field in the substrate steers the charge carriers to the potential wells with minimal loss of spatial resolution.

This type of CCD has several advantages over thinned CCDs. Since the electric field extends to the backside contact, the device does not require thinning, resulting in simpler packaging. As

already discussed, the thicker active region results in optical response nearly to the silicon bandgap cutoff at 1100 nm and x-ray response to about 13 keV.

In order to realize the benefits of such a CCD, several technical challenges needed to be overcome. One concern was maintaining low dark currents with a substantially thicker depletion region as compared to thinned CCDs. A technique for processing high-resistivity silicon while maintaining low dark currents had been previously developed for high-energy physics detectors [35], and this active gettering technique was also used for the CCD fabrication. It consists of the deposition of a phosphorus-doped, backside polycrystalline silicon layer which getters harmful impurities during the fabrication process. High dark currents were a significant problem with initial attempts to develop CCDs on high-resistivity substrates [36,37].

Another significant challenge was the development of a transparent back-side window that allows transmission of short-wavelength light and application of the bias voltage necessary for full depletion of the substrate. A backside window consisting of a thin layer of in-situ doped polysilicon with an indium-tin oxide antireflection coating was developed [1,27].

vi. Planned development

Current development objectives are:

1. Device physics issues/optimization of CCD characteristics
2. Process technology development
3. Commercialization

In the device physics area several studies are being investigated. The main CCD parameters to be optimized are quantum efficiency, read noise, charge transfer efficiency, dark current, and full well capacity. For the most part these have been characterized on the 200×200 prototypes, but in some cases there is room for improvement. In other cases scale up to large area devices must be demonstrated (especially dark current).

Fabrication runs using the recently acquired 1:1 scanning lithography system will be used for the CCD optimization studies. Figure 4 shows the mask design used for the current fabrication run. Included in this design are CCDs varying in size from 200×200 to 2048×2048 , transistor test structures of varying geometry, p-i-n diode test structures, interpoly oxide capacitor test structures, contact resistance test structures, and in-process monitors for alignment characterization. Within a lot of 20 wafers, the lot is split and only a small subset of wafers are fully processed to completion at any time so that the effect of critical process steps can be fully assessed.

All of the larger CCDs shown in Fig. 4 have split vertical registers to allow for either frame store or frame transfer operation. The serial registers are also split to allow for two readout amplifiers per CCD. The four 512×512 CCDs have output transistors of different geometry to investigate possible improvements in noise when compared to the 200×200 prototype. Also included are high frame rate CCDs that are prototype devices for the JPL Space Interferometry Mission (SIM). These CCDs have four amplifiers (1 for every 32 columns) for fast readout in a 128×32 , $24 \mu\text{m}$ pixel format.

High quantum efficiency across a wider wavelength range than is possible with conventional CCDs is one of the major advantages of this type of CCD. However, the QE at present is limited by the single layer, indium tin oxide anti-reflection coating. We intend to develop improved coatings based on two-layer coatings consisting of sputtered silicon dioxide and indium-tin oxide layers. Detailed design studies are required for proper optimization of the two-layer system, followed by actual implementation. In particular, increased QE in the near IR is the major goal of this work.

Fabrication of CCDs on high resistivity, float zone silicon is complicated by the enhanced susceptibility of dislocation generation during high temperature processing in such material [Gregory]. Dislocations are generated as a result of the thermal gradients present during temperature ramping. If significant problems are found a detailed characterization of the thermal gradients

present during wafer furnace operations may be required. Commercially available thermocouple-instrumented wafers could be used to realize furnace conditions that result in minimal thermal gradients.

Concurrent with the process technology development and the fabrication of large-format devices we intend to bring the process of transferring the process technology to a commercial vendor. Commercialization will require further optimization and refinement of the process recipes.

vii. Lateral diffusion

In the case of a fully-depleted, back-illuminated CCD, there was some concern that lateral diffusion of the charge might be important, during its transit from production near the back surface to the potential wells located nearly 300 μm away. This has been studied in detail both theoretically and experimentally [3].

Expressions for charge spreading, in a gaussian approximation in which longitudinal diffusion was ignored, were derived in the case of an overdepleted substrate. The transit time of carriers in an electric field is calculated, and the rms deviation in x and y due to diffusion is then given by $\sqrt{2D t_{\text{tr}}}$ where D is the diffusion coefficient and t_{tr} is the carrier transit time. For the electric field profile in a p-i-n diode (which matches that in a CCD except near the potential wells) the result is

$$\sigma_{od} = \sqrt{2D t_{\text{tr}}} = \sqrt{2 \frac{kT}{q} \frac{\epsilon_{\text{Si}}}{\rho_n} \ln \frac{E_{\text{max}}}{E_D}} \xrightarrow{V \rightarrow \infty} \sqrt{2 \frac{kT}{q} \frac{y_D^2}{V}} \quad (1)$$

where k is Boltzmann’s constant, T is the temperature in Kelvin, q is the electronic charge, ϵ_{Si} is the permittivity of silicon, $\rho_n = qN_D$ is the volume charge density in the depleted region where N_D is the donor atom density in the depleted region, E_{max} is the field at the p-n junction, and E_D is the field at y_D , where the backside contact is located. y_D is essentially the thickness of the substrate. An implicit assumption used in deriving Eq. (1) is that the photons are absorbed at y_D , which is the worst case. A more general derivation would lead to E_D in the above equation being replaced by $E_{\text{max}} + (\epsilon_{\text{Si}}/\rho_n)y$, where y is the depth at which the photon is absorbed. At high fields σ_{od} approaches the constant-field result indicated by the limit $V \rightarrow \infty$ in Eq. (1), where V is the applied potential. The standard deviation is independent of N_D and linear in y_D , the substrate thickness.

If part of the substrate is undepleted, lateral diffusion is dominated by diffusion in this field-free region. There is a related potential problem, and the results, while complicated, are well-known. The distribution has significant nongaussian tails, and the standard deviation is given by $0.8616 y_{ff}$, where y_{ff} is the thickness of the field-free region.

Charge diffusion was experimentally characterized by imaging a pinhole mask consisting of small openings etched in a chrome layer on a quartz substrate that is placed directly on a back-illuminated CCD [2,3]. A filter centered at 400 nm was used to give short-wavelength light which is absorbed within 0.1–0.2 μm from the surface. Figure 8 shows the measured rms charge spreading as a function of substrate bias voltage. At large bias voltages the rms charge spreading is about 10 μm , which is negligible in many astronomical applications. According to the field-free diffusion analysis, a similar amount of charge spreading is expected in a thinned CCD with about 11 μm of field-free region [39].

viii. Radiation hardness

Radiation damage is relevant to future space applications. J. Janesick has been pointed out (private communication) that the major bulk damage effect due to space protons, for example, is the generation of trapping states due to formation of phosphorus-vacancy pairs (the P-V center) [15,40,41,42,43]. This defect results in hot pixels (high dark current) and degrades CTE.

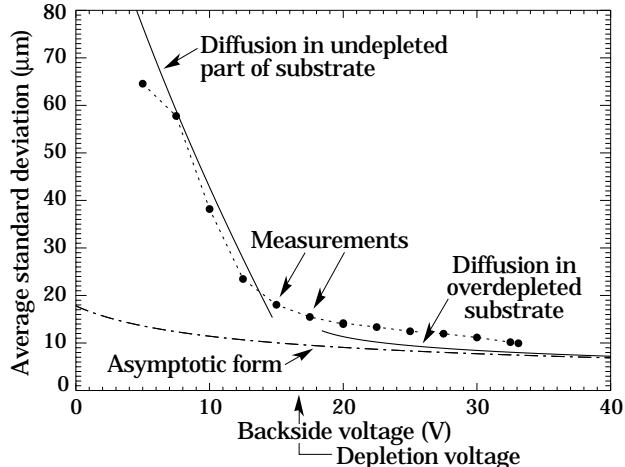


Figure 8: Measured rms lateral diffusion (x or y) for point sources of blue light on the back of an UCB/LBNL CCD. In the present analysis, undersampling results in an overestimate for $\sigma \lesssim 15 \mu\text{m}$. The expressions given in Eq. (1) for the overdepleted and asymptotic forms are plotted, as is the analytic result in the case of dominance of diffusion in the field-free region.

Typical CCDs have phosphorus implanted channels, with peak phosphorus concentrations in the low 10^{16} cm^{-3} range [38]. Our p-channel CCD has a boron implanted channel, and the background phosphorus concentration is extremely small in the high-resistivity substrate (in the low 10^{11} cm^{-3} range). Therefore it is expected that P-V centers will not limit radiation hardness, but instead oxygen-related defects as observed by Meidinger *et al.* [44]. High-resistivity silicon has significantly reduced oxygen levels as well [45]. The type of CCD under development here has already been shown to have significantly improved radiation hardness when compared to conventional CCDs.

ix. Conclusion

CCDs are used in a wide range of instruments. Over the past decade charge-coupled device (CCD) detectors have launched a revolution in observational astronomy. The two orders of magnitude improvement in quantum efficiency compared to the photographic plates, and the almost six orders of magnitude increase in number of resolution elements compared to a photomultiplier have enabled research once only dreamt of.

The goals in developing new CCDs are essential two-fold: to enable new science, and to significantly improve the quality and quantity of data for all types of science. Examples of science-driven CCD detector improvements include, as an example, the considerable effort which has gone into the thinning of the CCD silicon substrate. Likewise considerable work has been performed to reduce readout noise and increase charge transfer efficiency, making CCDs useful for very low-light applications such as spectroscopy, narrow-band imaging, imaging in space, and high-speed photometry. CCDs have been made larger so that more, or larger, objects or spectral elements can be observed in one exposure. Indeed, a number of instruments using mosaics of CCDs (up to 8k x 10k pixels and more) have been developed in the last few years which have allowed surveys with sky coverage approaching that attained when photographic plates were in use. The quantum efficiency has been improved through the use of thinning and anti-reflection coatings, again improving the quality of the scientific data.

Despite these impressive developments, the shortcomings of modern CCDs are not negligible. The thinning process employed to enhance UV response results in decreased red response since for thin CCDs the product of the silicon absorption cross-section and the thickness becomes less than one as the band-gap energy is approached. This not only results in lower red quantum efficiency,

but fringes develop as transmitted photons are reflected with a thinned CCD and subsequently interfere with incoming photons. High quantum efficiency from the UV to 1000 nm, and without fringing, is an important goal for CCD detector development and would revolutionize the field.

The “fully-depleted” CCDs will substantially extend the reach of astronomers in several respects: High-performance CCDs will be available at a reasonable cost to astronomers working at smaller facilities, and the extra near-infrared capability will greatly facilitate spectroscopic and high red-shift studies in optical astronomy.

Our CCD is well suited to space- and ground-based telescope applications that require:

- o Optical and near-IR coverage with a single camera package.
 - Large telescopes cannot change instruments quickly.
 - Space-based telescopes cannot always afford the weight and complexity of secondary systems.
 - Spectroscopy and imaging often need continuous high-efficiency from optical to near-IR.
- o Reasonable cost imagers.
 - Avoiding expensive very cold temperature overhead, and expensive IR detectors.
 - Large mosaic focal plane coverage with reasonable cost and complexity.
 - Direct chip-for-chip replacement in current CCD cameras and spectrographs to allow retrofit
- o Radiation hardness for space-based applications.

These instrumental requirements are demanded by a large fraction of upcoming cosmology projects, since the wavelengths of interest are typically just in the crossover between optical and near-IR. New instruments designed specifically to take advantage of the “fully-depleted” thick high-resistivity CCDs characteristics are likely to become mainstream scientific tools.

III. References

1. S.E. Holland *et al.*, “A 200×200 CCD image sensor fabricated on high-resistivity silicon,” IEDM Tech. Digest, 911, 1996.
2. R. Stover *et al.*, “Characterization of a fully-depleted CCD on high resistivity silicon,” *Solid State Sensor Arrays: Development and Applications*, Proceedings of SPIE **3019**, 183-188, 1997.
3. S.E. Holland *et al.*, “Development of back-illuminated, fully-depleted CCD image sensors for use in astronomy and astrophysics,” *1997 IEEE Workshop on Charge-Coupled Devices and Advanced Image Sensors*, Bruges, Belgium, 1997.
4. Webpage for CCD development at UCB/LBNL is <http://design.lbl.gov/CCD/>.
5. J. Janesick, “CCDs: The inside story,” *CCD Astronomy*, 10–15, Winter 1997.
6. S. M. Sze, *Physics of Semiconductor Devices*, 2nd Edition, p. 15, Wiley, 1981.
7. B.E. Burke *et al.*, “Soft-X-Ray CCD imagers for AXAF,” *IEEE Trans. Elec. Dev.*, **44**(10), pp. 1633-1642, October 1997.
8. B.E. Burke, R.W. Mountain, P.J. Daniels, M.J. Cooper, and V.S. Dolat, “CCD soft x-ray imaging spectrometer for the ASCA satellite,” *IEEE Trans. Nucl. Sci.*, **41**(1), 375–385, Feb. 1994.
9. B.E. Burke, R.W. Mountain, D.C. Harrison, M.W. Bautz, J.P. Doty, G.R. Ricker, and P.J. Daniels, “An abutable CCD imager for visible and x-ray focal plane arrays,” *IEEE Trans. on Electron Devices* **38**(5), 1069–1076, May 1991.
10. P.S. Heyes, P.J. Pool, and R. Holton, “A new generation of scientific CCD sensors,” *Solid State Sensor Arrays: Development and Applications*, Proceedings of SPIE, pp. 201-209, 1997.

11. A.D. Holland, "CCDs for future X-ray astronomy missions," EUV, X-Ray and Gamma-Ray Instrumentation for Astronomy VIII, Proc. of SPIE, **3114**, pp. 586-597, 1997.
12. A.D. Holland, "X-ray spectroscopy using MOS CCDs," Nucl. Instruments and Methods in Physics Research, **A337**, pp. 334-339, 1996.
13. D.H. Lumb, "Applications of charge-coupled devices to x-ray astrophysics missions," Nucl. Instruments and Methods in Physics Research, **A288**, pp. 219-226, 1990.
14. D.H. Lumb, E.G. Chowanietz, and A. Wells, "X-ray measurements of charge diffusion effects in EEV Ltd. charge coupled devices," Optical Eng., **26**(8), pp. 773-778, August 1987.
15. J. Janesick, G. Soli, T. Elliot, and S. Collins, "The effects of proton damage on charge-coupled devices," Charge-Coupled Devices and Solid State Optical Sensors II, Proc. of SPIE, **1447**, pp. 87-108, 1991.
16. C. von Zanthier *et al.*, "A 6 cm \times 6 cm fully depleted pn-junction CCD for high resolution spectroscopy in the 0.1 keV to 15 keV photon energy range," Solid State Sensor Arrays: Development and Applications II, Proceedings of SPIE, pp. 27-36, 1998.
17. P. Holl *et al.*, "A 36 cm² large monolithic pn-CCD detector for EPIC on XMM," EUV, X-Ray and Gamma-Ray Instrumentation for Astronomy VIII, Proc. of SPIE, **3114**, pp. 126-133, 1997.
18. L. Strüder *et al.*, "A 36 cm² large monolithic pn-CCD detector for X-ray astronomy," 1997 IEEE Workshop on Charge-Coupled Devices and Advanced Image Sensors, Bruges, Belgium, 1997.
19. H. Soltau *et al.*, "Performance of the pn-CCD X-ray detector system designed for the XMM satellite mission," Nucl. Instruments and Methods in Physics Research, **A337**, pp. 340-345, 1996.
20. H. Bräuninger *et al.*, "First results with the pn-CCD detector system for the XMM satellite mission," Nucl. Instruments and Methods in Physics Research, **A326**, pp. 129-135, 1993.
21. L. Strüder *et al.*, "The MPI/AIT x-ray imager (MAXI)-high speed pn CCDs for x-ray detection," Nucl. Instruments and Methods in Physics Research, **A288**, pp. 227-235, 1990.
22. L. Strüder, P. Holl, and G. Lutz, "Development of fully depletable CCDs for high energy physics applications," Nucl. Instruments and Methods in Physics Research, **A257**, pp. 594-602, 1987.
23. M. Lumb, H. Eggel, R. Lainé, and A. Peacock, "X-ray multi-mirror mission - an overview," EUV, X-Ray and Gamma-Ray Instrumentation for Astronomy VII, Proc. of SPIE, **2808**, pp. 326-337, 1996.
24. R. Hartmann, L. Strüder, J. Kemmer, P. Lechner, O. Fries, E. Lorenz, and R. Mirzoyan, "Ultrathin entrance windows for silicon drift detectors," Nucl. Instruments and Methods in Physics Research, **A387**, pp. 250-254, 1997.
25. R. Stover, private communication; also see, <http://gardiner.ucolick.org:80/~ccdev/lincoln>.
26. M.M. Blouke and M.D. Nelson, "Stable ultraviolet antireflection coatings for charge-coupled devices," *Charge-Coupled Devices and Solid State Optical Sensors III*, Proceedings of SPIE **1900**, 228-240, 1993.
27. S.E. Holland, N.W. Wang, and W.W. Moses, "Development of low noise, back-side illuminated silicon photodiode arrays," IEEE Trans. Nucl. Sci., **44**(3), pp. 443-447, June 1997.
28. Klaus Hodapp, private communication. Also see <http://www.ifa.hawaii.edu/instrumentation/quirc/quirc.html>, and K. Hodapp *et al.*, *New Astronomy* **1**(2):177-196, November 1996.

29. M. P. Lesser and B.L. McCarthy, "Quantum efficiency characterization of scientific CCDs", *Solid State Sensor Arrays and CCD Cameras*, Proceedings of SPIE, **2654**, 1996.
30. J. Janesick, "CCD transfer method: standard for absolute performance of CCDs and digital CCD camera systems," *Solid State Sensor Arrays: Development and Applications*, Proc. SPIE, 70–103, 1997.
31. R.J. Stover *et al.*, "A high performance CCD on high resistivity silicon," to be published in *Remote Sensing of the Atmosphere, Environment, and Space*, Proceedings of SPIE, **3505**, 1998.
32. S.R. Kamasz, M.G. Farrier, and C.R. Smith, "Characterization and modeling of CCD devices on high-resistivity silicon substrates," *Charge-Coupled Devices and Solid State Optical Sensors IV*, Proceedings of SPIE **2172**, 76–87, 1994.
33. H.Y. Tsoi, J.P. Ellul, M.I. King, J.J. White, and W.C. Bradley, "A deep-depletion CCD imager for soft x-ray, visible, and near-infrared sensing," *IEEE Trans. Electron Devices* **32**(8), 1525–1530, August 1985.
34. Technology Modeling Associates, Inc.
35. S. Holland, *Nucl. Instrum. Meth.* **A275**, 537 (1989).
36. D.M. McCann *et al.*, "Area array x-ray sensors," *Advances in Focal Plane Technology*, Proc. of SPIE **217**, 118–128, 1980.
37. M.C. Peckerar, D.H. McCann, and L. Yu, *Appl. Phys. Lett.* **39**(1), 55–57, July 1981.
38. J. Janesick, T. Elliot, R. Winzenread, J. Pinter, and R. Dyck, "Sandbox CCDs," *Charge-Coupled Devices and Solid State Optical Sensors V*, Proc. SPIE **2415**, 1995.
39. <http://sauron.as.arizona.edu/ccdlab/>.
40. J. Janesick, T. Elliot, and F. Pool, "Radiation damage in scientific charge-coupled devices," *IEEE Trans. Nucl. Sci.* **36**(1), 572–578, Feb. 1989.
41. A. Yamashita *et al.*, "Radiation damage to charge-coupled devices in the space environment," *IEEE Trans. Nucl. Sci.*, **44**(3), pp. 847-853, June 1997.
42. A. Holmes-Siedle, A. Holland, and S. Watts, "The impact of space protons on x-ray sensing with charge coupled devices (CCDs)," *IEEE Trans. Nucl. Sci.*, **43**(6), pp. 2998-3004, December 1996.
43. G.R. Hopkinson, C.J. Dale, and P.W. Marshall, "Proton effects in charge-coupled devices," *IEEE Trans. Nucl. Sci.*, **43**(2), pp. 614-626, April 1996.
44. N. Meidinger, L. Strüder, H. Soltau, and C. v. Zanthier, "Radiation hardness of pn-CCDs for X-ray astronomy," *IEEE Trans. Nucl. Sci.* **42**(6), 2066–2073, December 1995.
45. W. von Ammon and H. Herzer, "The production and availability of high resistivity silicon for detector applications," *Nucl. Instrum. Meth.* **A226**, 94–102, 1984.